Cis-4-[^{18}F]Fluoro-L-Proline PET Imaging of Pulmonary Fibrosis in a Rabbit Model

William E. Wallace, PhD[1]; Naresh C. Gupta, MD[2]; Ann F. Hubbs, DVM, PhD[1]; Samuel M. Mazza, PhD[2]; Harry A. Bishop, MD[2]; Michael J. Keane, MS[1]; Lori A. Battelli, BS[1]; Jane Ma, PhD[1]; and Patricia Schleiff, MS[1]

[1]National Institute for Occupational Safety and Health (NIOSH), Centers for Disease Control and Prevention (CDC), Morgantown, West Virginia; and [2]West Virginia University PET Center, Morgantown, West Virginia

A fluorinated analog of proline amino acid, cis-4-[^{18}F]fluoro-L-proline (FP), was tested for potential use in PET for detection and evaluation of pulmonary response to respirable crystalline silica. The purpose of the study was to determine whether PET imaging with FP is sensitive for detection of pulmonary fibrosis. **Methods:** Experimental silicosis was produced in rabbits by airway instillation of 300 mg respirable silica in 0.9% sterile saline; control rabbits received only saline. After 1, 2, 4, or 5 mo, animals were injected with 37 MBq (1 mCi) FP, and imaged in sets of 2 to 3 in a PET scanner using a dynamic scanning protocol over a 3-h period. Each imaging set contained at least 1 control rabbit. FP uptake in each lung was scored from 0 to 5 (PET score) by consensus of 3 readers blinded to animals' exposure status. Animals were humanely killed 2 d after the last imaging, and tissue sections from each lung lobe were graded from 0 to 5 by histopathology examination (histopathology score) for severity and distribution of fibrosis. **Results:** Silicotic animals had significantly higher ($P < 0.05$) PET scores at each time point than did control animals. Repeated-measures ANOVA showed significant differences in PET scores between silicotic and control animals for the total lung field, but there were no statistically significant time trends for either group. Presence of fibrosis (i.e., histopathology score > 1) showed a significant association with elevated PET score (i.e., PET score > 1) using Fisher's exact test ($P < 0.05$). PET scores also showed excellent predictive ability, as all animals (18/18) with fibrosis also had elevated PET scores, and 95% (18/19) of animals with PET scores > 1 showed evidence of fibrosis. Localization of activity to specific lung areas was less exact, perhaps due in part to the small animal size for the resolution of the clinical PET imager used. PET scores were elevated (>1) for 67% (10/15) of silicotic right lungs and 75% (12/16) of silicotic left lungs; fibrosis scores > 1 were measured in 91% (10/11) of right lungs with PET scores > 1, and in 92% (12/13) of such left lungs. **Conclusion:** The FP tracer provided sensitive and specific identification of silicotic animals in early stages of the disease. This suggests that FP PET imaging has the potential sensitivity to detect active fibrosis in silicosis and other lung diseases. Additional studies are needed to determine the specificity of the FP tracer for fibrosis versus inflammatory processes.

Key Words: PET; fluoro-L-proline; silicosis; pulmonary fibrosis

J Nucl Med 2002; 43:413–420

Occupational pneumoconioses were responsible for over 3,000 deaths in the U.S. in 1996 (*1*). Silicosis, one of the pneumoconioses, continues to plague workers in some occupations, e.g., surface mining, despite occupational exposure regulations and the availability of exposure prevention measures (*2*). PET uses radiopharmaceuticals to produce images of metabolic activity and so offers the possibility for detection of early biochemical changes that occur in pneumoconioses. This could permit earlier detection, more timely direction of preventative actions, and more rapid and definitive grading and therapy evaluation for management of advancing stages of the disease than are afforded by chest radiography (*3*).

Even when clinical indications of pulmonary fibrosis are minimal, excess collagen is found in the alveolar wall in early disease, over a background of ongoing equilibrium of collagen synthesis and degradation (*4–6*). Increased lung hydroxyproline content is associated with development of silicotic nodules in rat lung, with increased rates of collagen synthesis seen within 2 wk of a single silica dust challenge (*7–10*). Incubation of embryonic cartilage with cis-4-fluoro-L-proline leads to incorporation of the analog in place of proline into an abnormal protocollagen and subsequently into abnormal collagen, which is retained intracellularly and not extruded into the extracellular matrix (*11*).

Thus, positron-emitter analogs of proline, [^{11}C]-L-proline or [^{18}F]fluoro-L-proline, may be accumulated in association with active fibrosis in pulmonary tissue. Wester et al. (*12*) measured the kinetics of in vivo uptake of cis- and trans-4-[^{18}F]fluoro-L-proline in mice bearing osteosarcomas, using γ-counting of necropsied tissue from animals killed between 5 min and 4 h after tracer injection. After 2 h, 70% of the activity of extracted cis-isomer was protein-bound, indicating that isomer may be suitable for evaluation of abnormal collagen synthesis. PET imaging for

Received Aug. 14, 2001; revision accepted Dec. 3, 2001.

For correspondence and reprints contact: Naresh C. Gupta, MD, WVU PET Center, P.O. Box 9236, Health Sciences Center South, Morgantown, WV 26505.

E-mail: ngupta@wvu.edu

in vivo pulmonary physiology and biochemistry studies has been reviewed (*13–15*). Traditional PET imaging using 2-[^{18}F]fluoro-2-d-deoxyglucose (FDG) as a tracer for glucose utilization has been found to be useful in characterizing chest tumors based on their level of metabolic activity, with a high degree of accuracy in differentiating benign from malignant pulmonary nodules. Glucose uptake is elevated in malignant tissue, and also in some active inflammatory processes (*16*,*17*). In a clinical study of PET imaging of the lung using [^{11}C]-L-methionine for tumor detection, an image of a large silicotic nodule was obtained and presumed to be associated with increased protein synthesis (*18*).

The objectives of the current study were to determine if PET imaging can detect heightened pulmonary uptake of cis-4-[^{18}F]fluoro-L-proline (FP) in the lungs of rabbits challenged with 300 mg crystalline silica instilled in the airway, and to compare FP PET images with histopathology data on the severity and distribution of fibrosis in lung necropsied after completion of PET imaging. The rabbit is a well-established silicosis animal model (*19–21*) with a large enough lung field to be resolved by PET imaging, although not large enough to clearly resolve PET features to smaller areas such as individual lung lobes. This allows us to address the first of two fundamental questions regarding the use of FP PET imaging for detection or evaluation of pulmonary fibrosis in an animal model: Is the rate of FP uptake associated with the disease process sufficiently above the background collagen synthesis rate to permit detection of fibrosis by PET imaging?

MATERIALS AND METHODS

Silica Challenge

We used a modification of a previously described rabbit model of unilateral silicosis (*19–21*). Specific-pathogen-free young adult (2.6–3.8 kg) male New Zealand White rabbits (Covance, Denver, PA) were anesthetized by intramuscular injection of ketamine and xylazine. The arytenoid folds of the larynx were identified using a pediatric laryngoscope, and an endotracheal tube was inserted into the trachea. The anesthetized rabbit was then placed in right lateral recumbency, and 1-mm tubing (Tygon; Saint Gobain Performance Plastics, Wayne, NJ) was blindly passed through the endotracheal tube until impedence was felt. Through the tubing, the airway was instilled with either 300 mg of respirable crystalline silica (Min-U-Sil; U.S. Silica, Berkeley Springs, WV) in 3 mL 0.9% sterile saline as a vehicle (silicotic animals), or saline alone (control animals). This localized the initial instillation to 1 lung lobe. Subsequent animal cough and aspiration could redistribute the silica between the lungs. Silicotic and control rabbits were randomly assigned to 3 groups: (a) imaging and necropsy 1 mo after instillation (9 rabbits); (b) serial imaging 1 and 2 mo after instillation and necropsy 2 mo after instillation (9 rabbits); and (c) serial imaging at 1, 2, 4, and 5 mo after instillation and necropsy 5 mo after instillation (12 rabbits).

Preparation of PET Radiotracer

FP was prepared stereospecifically in a semiautomated system using a quaternary 4-aminopyridinium resin to effect ^{18}F fluorination (*22*). The p-tosyloxy moiety of N-t-butoxycarbonyl-trans-4-p-tosyloxy-L-proline methyl ester was displaced with [^{18}F]fluoride. Then the carbamate moiety was hydrolyzed with dilute aqueous HCl, and the methyl ester was hydrolyzed with dilute aqueous NaOH. Finally, the pH was adjusted with phosphate buffer. Radiochemical purity was >99%.

PET Imaging

At intervals of 1, 2, 4, and 5 mo after instillation, animals were anesthetized with ketamine, xylazine, and acepromazine and injected intravenously with 18.5–37.0 MBq FP. Two to three animals were injected and imaged simultaneously in a PET scanner (Advance; GE, Wakeshaw, WI), with 1 control animal in each imaging group to provide a direct comparison of animals and imaging conditions, differing only in silica challenge. Transmission imaging was performed before the start of emission scanning, using an external radiation source for tissue attenuation corrections of emission data. This also provided for anatomical localization of emission features by overlay of transmission and emission images. PET scanning used a dynamic scanning protocol of 11 × 10 s, 5 × 20 s, 3 × 30 s, 3 × 5 min, 2 × 10 min, and 6 × 20 min, for a total scanning time of 3 h. Static images from the last 20-min imaging period were scored for FP uptake seen in transverse views of the lungs, and only these data were statistically analyzed in the current report. Activity was localized to the extent possible to right (R) or left (L) lung or mediastinum, and anterior, posterior, superior, or inferior locations in each lung by digital overlay fusion of the emission images with transmission images using an image registration program. Figure 1 shows such cross-sectional lung images (emission, transmission, and overlay images) from a silicotic rabbit; Figure 2 shows images from a control animal.

PET images were scored for intensity of FP uptake (PET score) by consensus of 3 readers blinded to the identity of the control animal. FP uptake intensity was scored from 0 (no discernable uptake) to 5 (multiple areas of intense tracer uptake). Readers viewed a complete set of 10 transaxial images from apex to the base of the lungs and subsequently assigned PET scores to each lung location.

In the first group of rabbits, 6 silicotic and 3 control animals were imaged at 1 mo after instillation and then humanely killed for histopathology examination (1 silicotic rabbit died after scanning and was not necropsied.) In the second group of rabbits, 6 silicotic and 3 control animals were imaged at 1 and 2 mo and then killed for histopathologic evaluation. In the third group of rabbits, 4 silicotic and 4 control animals were imaged at 1, 2, 4, and 5 mo and then killed for histopathologic evaluation (4 additional silicotic rabbits died after scanning: 1 died at 1 mo, and 3 died at 4 mo after instillation; the latter 3 were necropsied).

Additionally, to see if subjectively identified anomalies had objectively measurable radioactivity levels above background, absolute uptake values of radiotracer activity per unit volume (Bq/mL) were calculated for lesion and background areas in 4 silicotic and 2 control animals at 30, 60, 120, and 150 d, and for 2 silicotic and 1 control animal at 30, 60, and 120 d by region of interest analysis. In silicotic animals with PET scores > 1, the radiotracer uptake indices (activity/unit volume) for a primary lesion were compared with the background uptake score from a contralateral lung area.

Histopathological Examination

To minimize radiation exposure of laboratory personnel, lungs were collected for histopathology 2 d after PET scanning (with the exception of 1 silicotic rabbit in the 1-mo group, which recovered

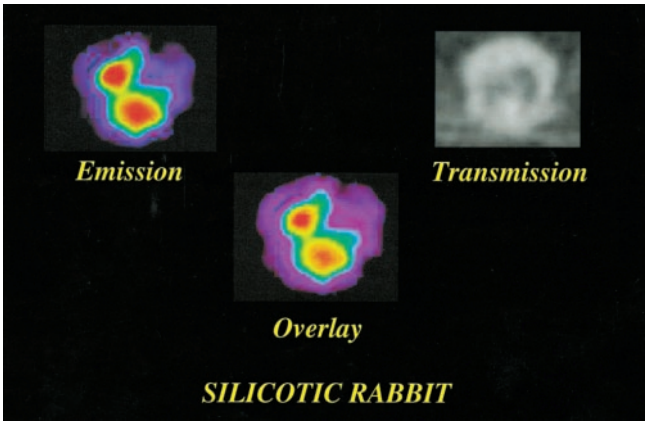

FIGURE 1. Transverse lung images of silicotic rabbit 120 d after silica challenge. Emission image and transmission image are overlaid to anatomically localize FP emission. Enhanced FP uptake is seen in L lung and heart (bottom center). Animal spine is at top; R lung is to R side. (PET scores and histopathology scores for this animal are listed in Table 1, row 25.)

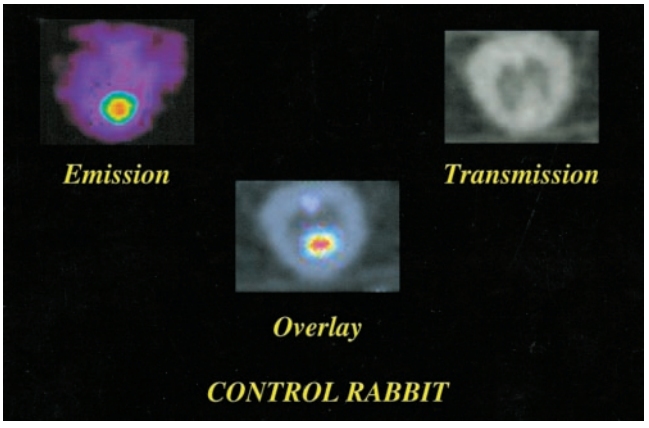

FIGURE 2. Transverse lung images of control animal 120 d after saline challenge. Emission image and transmission image are overlaid to anatomically localize FP emission. Enhanced FP uptake is seen in heart (bottom center). (PET scores and histopathology scores for this animal are listed in Table 1, row 18.)

poorly from anesthesia and was humanely killed 1 d after scanning). This 2-d wait for necropsy should result in insignificant changes in histopathology scores for animals instilled with silica at least 1 mo previously. Rabbits were killed by intravenous injection of an overdose of sodium pentobarbital; this was followed by exsanguination. The lungs were then airway-perfused with 60 mL of 10% neutral buffered formalin. Tissues were routinely processed, paraffin-embedded, and sectioned at 5 μm. Optical microscopy examination was performed on hematoxylin and eosin and trichrome stained sections from each lung lobe: R and L apical (Ra, La), R and L cardiac (Rc, Lc), R and L diaphragmatic (Rd, Ld), and the azygous lobe when present (az). Fibrosis was visualized using trichrome staining for collagen detection. Figure 3 shows photomicrographs of lung tissue from a silicotic animal displaying a silicotic nodule and from a control animal showing normal pulmonary alveolar structure. Sections were scored for fibrosis on a 0–5 scale for distribution and a 0–5 scale for severity as previously described (*23*). Distribution was scored as follows: focal = 1; locally extensive = 2; multifocal = 3; multifocal and coalescent = 4; and diffuse = 5. Severity was scored as follows: minimal = 1; mild = 2; moderate = 3; marked = 4; and severe = 5. For statistical analyses, an overall score (histopathology score) was created for each lung lobe by adding the distribution and severity scores. If either the severity score or distribution score was ≤1, then the lobe histopathology score was set at 0 in statistical analyses of the data.

Data Analysis

The following hypotheses were tested:

1. Animals instilled with respirable crystalline silica will have higher pulmonary uptake of FP as observed by PET imaging than control animals.

2. Animals with positive uptake of FP in the lungs and a PET score of >1 will have a higher histopathology score overall and for any location in the lung.

3. Animals with positive uptake of FP in the lungs and a PET score of >2 will have a higher histopathology score overall and for any location in the lung.

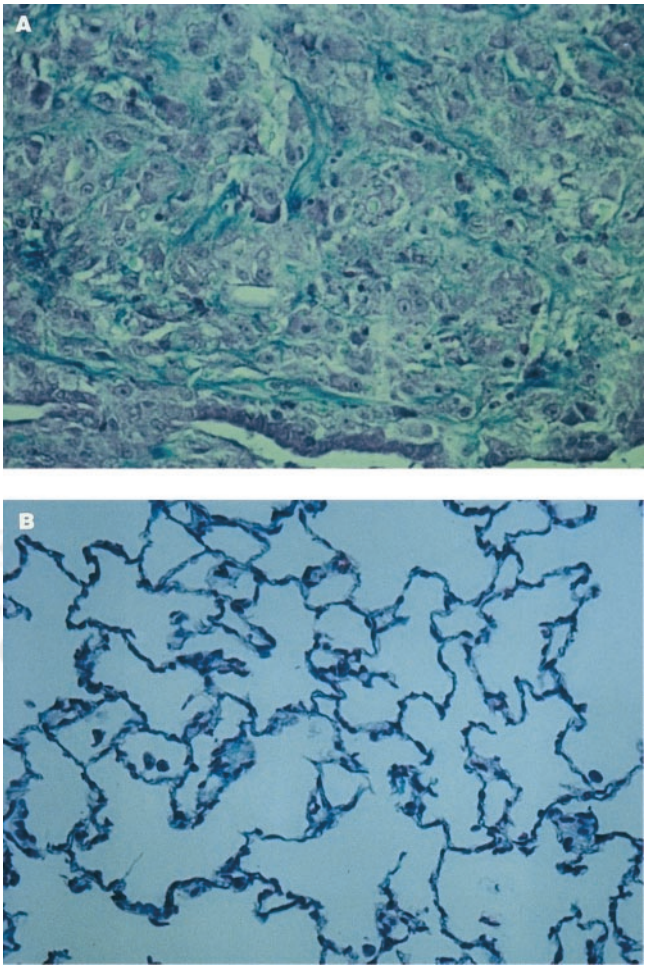

FIGURE 3. Histopathology cross-sectional microscopy images of lung tissue from silicotic (A) and control (B) rabbit. Control lung shows normal pulmonary alveoli with no thickening of septa. Silicotic lung shows extracellular collagen (blue stain) in a lung nodule. 1 cm = approximately 50 μm.

4. In animals instilled with respirable crystalline silica, lower PET scores will correspond to lower histopathology scores, and higher PET scores will correspond to higher histopathology scores.

Statistical analyses, including the Wilcoxon rank-sum test, Fisher's exact test, and repeated-measures ANOVA, were performed to compare histopathology scores determined by histopathology examination with PET scores obtained by FP PET imaging. Statistical significance was achieved when the P value was <0.05.

For the first 3 hypotheses, an overall PET score was created by adding all 3 PET scores of the R lung, L lung, and mediastinum. For hypotheses 2–4, a final PET score was compared with the histopathology score for each animal. The highest histopathology score among the apical, cardiac, and diaphragmatic lobe scores for each lung was assigned as the histopathology score for the R and L lungs. For analyses of specific lung regions, a R lung PET score was created by adding the scores for the R lung and mediastinum, and a L lung PET score was created by adding the scores for the L lung and mediastinum. This was done because of the resolution of the PET images and small size of the animal lungs, which meant that PET-imaged regions of radiotracer accumulation sometimes could not be assigned to specific lobes within a lung; in particular, there was some ambiguity in assigning features located near the mediastinum. Additionally, some animals had an azygous lung lobe, which arises from the R bronchus but resides near the midline between the lungs. Therefore, the PET activities of the R lung or mediastinal region were compared with the histopathology sections of the R lung and azygous lobes; and the PET activities of the L lung or mediastinal region were compared with the histopathology sections of the L lung and azygous lobes. For hypothesis 4, the PET scores and histopathology scores were transformed into rank values, and Spearman's correlation coefficients were calculated to determine whether lower PET scores correspond to lower histopathology scores, and whether higher PET scores correspond to higher histopathology scores in silicotic animals.

The association of a significantly elevated PET score (>1 or >2) with histopathological evidence of significant fibrosis (histopathology score >1 for both distribution and severity), or the sensitivity of PET imaging for the detection of fibrosis, was determined for whole animals as the percentage of the animals with a significantly elevated pathology score for any lung lobe that also had a significantly elevated PET score anywhere in the lungs (R lung, L lung, or mediastinum). This comparison was made also for the individual R and L lung regions (when an azygous lobe was present, it was considered a component of both lungs for statistical purposes). The association of an absence of a significantly elevated PET score with an absence of fibrosis, or the specificity of PET imaging for the presence of fibrosis, similarly was determined for whole animals and for R and L lung regions.

RESULTS

Table 1 presents the PET scores for each animal at each imaging time including scores >1 (if any) for R lung, L lung, and mediastinum (M); and the histopathology scores >1 (if any) for each lung region. Histopathology scores are given as severity/distribution for each lung lobe. If either the severity or distribution score was ≤ 1, the scores were not considered as clearly indicative of disease, and were ascribed a value of 0 in the statistical analyses.

The results of testing the 4 hypotheses were as follows: The overall lung region of silicotic animals exhibited significantly higher uptake of FP, as scored on PET images, compared with control animals. Animals with PET scores of >1 had significantly higher histopathology scores overall, for the R lung region, and for the L lung region than did animals with lower PET scores. For silicotic animals, the association between higher histopathology scores and higher PET scores was statistically significant but not strongly so.

All silicotic animals except 1 had PET scores >1 at all 4 time points. The exception had a PET score of 0 at the first time point (1 mo), which evolved into high scores (4.5) at the 2 subsequent time points. All silicotic animals presented significant fibrosis in at least 1 lung lobe on histopathology examination. Among control animals, 1 animal had a PET score of >1 (1.5) at the final imaging point (5 mo); and 1 animal had a score of 2.5–3 in the early time points, which resolved to 0 at the final time point; all other control animals had PET scores of 0 or 1 at all time points. On histopathology, none of the control animals showed significant fibrosis (distribution and severity >1) in any lung lobe.

Figure 4 presents the median distribution with 25th and 75th quantiles of the additive PET scores for each silicotic and control animal at each imaging time. There was significantly greater FP uptake in lungs of silicotic animals compared with control animals. Wilcoxon rank-sum tests found significantly higher uptake by silicotic animals at 1, 2, 4, and 5 mo, with respective P values of 0.0001, 0.001, 0.02, and 0.03. Considering that the animals were imaged in 3 batches, there was no significant batch effect on treatment differences at each timed interval; all P values were >0.05.

Repeated-measures ANOVA of PET scores for the 8 animals that were imaged at all 4 time points showed clear evidence of treatment differences for the whole rabbit ($P = 0.0005$), but not for the R lung ($P = 0.05$), L lung ($P = 0.38$), or mediastinum ($P = 0.28$). Over time, the silicotic animals showed no significant increase in PET scores.

Table 2 shows the number of animals with each possible combination of positive and negative PET scores and histopathology scores, tabulated for the whole animal and for separate R and L lung regions. Histopathology scores with both severity and distribution >1 were considered positive. Tables were calculated defining PET scores >1 as positive, and also using >2 as positive. Animals with a PET score >1 had a positive overall histopathology score, with a P value of <0.005 for all tables as determined by Fisher's exact test. For the whole animal, there were no animals with a negative PET score and positive histopathology score (0/18); while 1 animal (1/10) with a negative histopathology score had a positive PET score. However, these correlations could not be resolved to specific lung regions: 33% of animals (5/15) with positive R lung fibrosis had negative PET scores; and 25% (4/16) with positive fibrosis had negative PET scores for the L lung region. For the R lung region, 9% (1/11) of

TABLE 1
PET and Histopathology Scores

	PET scores (lung area)				Histopathology scores (severity/distribution)						
	Months after challenge				Lung region						
	1	2	4	5	Ra	Rc	Rd	az	La	Lc	Ld
1. Control	0				0	0	0	0	0	0	0
2. Control	0				0	0	0	0	0	—	0
3. Control	0				0	0	0	0	0	0	0
4. Silicotic	2.5 (R) 2.5 (L)				2/3	2/4	2/3	2/2	—	0	2/3
5. Silicotic	3.5 (R) 2.5 (L)				0	2/3	—	0	2/3	—	2/3
6. Silicotic	4 (R)				2/3	2/4	2/3	—	—	0	—
7. Silicotic	3.5 (M)				—	2/3	2/4	2/5	0	0	0
8. Silicotic	4 (L)				—	—	0	0	0	—	2/4
9. Control	—	0			0	0	0	0	0	0	0
10. Control	0	0			0	0	0	0	0	0	0
11. Control	0	0			0	0	0	0	0	—	0
12. Silicotic	2.5 (R)	3 (R)			2/3	2/3	2/3	3/5	0	0	—
13. Silicotic	2.5 (R) 1.5 (L)	2.5 (L)			2/4	—	2/3	—	0	—	2/3
14. Silicotic	2.5 (L) 2.5 (M)	4.5 (L)			2/3	—	—	—	—	—	3/4
15. Silicotic	3.5 (L)	4.5 (L)			0	0	0	0	0	0	3/4
16. Silicotic	2.5 (R)	3.5 (L)			2/3	2/3	0	0	2/3	2/4	2/4
17. Silicotic	3.5 (R) 3.5 (L)	3.5 (L)			0	2/3	0	2/4	0	0	0
18. Control	0	0	—	0	0	0	0	0	0	0	0
19. Control	2.5 (R)	3 (R)	—	0	0	0	0	0	0	0	0
20. Control	0	0	0	1.5 (M)	0	0	0	0	0	0	0
21. Control	0	1.5 (R)	0		0	0	0	0	0	0	0
22. Silicotic	3.5 (R) 3.5 (M)	3.5 (R) 3.5 (M)	1.5 (R)	3.5 (R) 3.5 (M)	2/3	2/3	—	3/5	0	0	0
23. Silicotic	3 (R) 3 (M)	4 (R)	4.5 (R)	4 (R)	3/3	3/4	3/4	—	0	0	0
24. Silicotic	3.5 (R)	3 (R)	3.5 (R)	3 (R)	2/3	2/3	2/3	2/3	2/3	0	0
25. Silicotic	4.5 (L)	3.5 (L) 1.5 (R)	4.5 (L)	3.5 (L)	0	2/3	2/3	0	0	0	3/3
26. Silicotic	0	4.5 (L)	4.5 (L)		0	0	0	0	0	—	3/4
27. Silicotic	3 (R)	2.5 (R)	3.5 (R)		—	2/3	2/3	2/3	0	0	—
28. Silicotic	1.5 (M)	2.5 (L) 2 (R)	1.5 (R)		2/3	2/3	0	0	2/3	2/3	3/3

For PET scores, 0 indicates all lung regions were 0; a dash indicates some regions were >0 but none were >1. For histopathology scores, a dash indicates either severity or distribution was >0 but ≤1.

animals with positive PET scores had negative histopathology scores; and 8% (1/13) were so for the L lung region.

For silicotic animals there was a statistically significant relationship between PET scores and histopathology scores in the R lung (correlation coefficient, 0.51; $P = 0.03$) and in the L lung (correlation coefficient, 0.66; $P = 0.003$), reflecting that higher histopathology scores were observed as PET scores increased.

In the limited PET image analyses using quantitative values of radiotracer activity, the average lesion-to-background uptake ratio for the 21 silicotic animals at each time point was 1.92:1 with a range of 2.70–1.25. For the 10 control animals at each time point with PET scores of <1 for all lung regions and times, the average absolute ratio between 2 separate background regions of the same animal was 1.19:1 with a range of 1.51–1.05. One control animal with a PET score of 1.5 at the final time point had a quantitative lesion-to-background uptake ratio of 1.75.

DISCUSSION

FP PET imaging exhibited high sensitivity and specificity for the whole animal, defining sensitivity as the percentage of fibrotic animals that had significant PET scores in either lung area, and defining specificity as the percentage of nonfibrotic animals with nonsignificant PET scores. How-

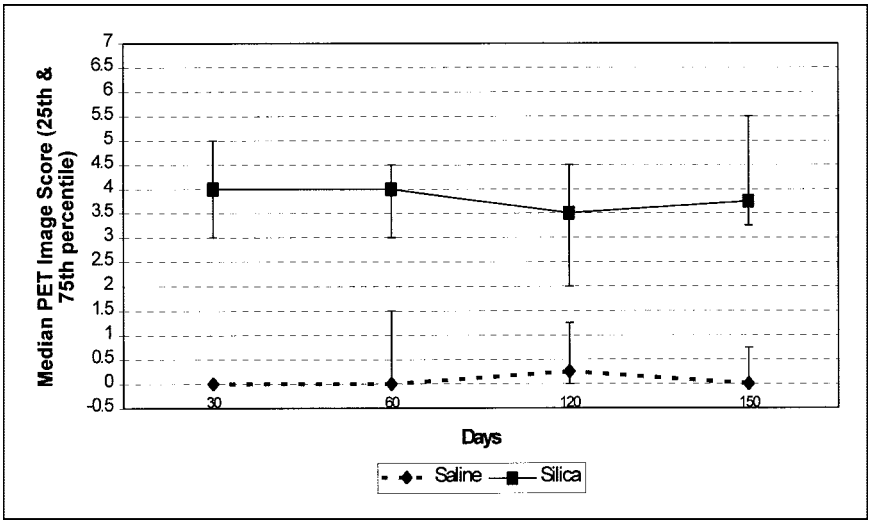

FIGURE 4. Median PET scores for all silicotic and control animals over time. Bars represent 25th and 75th quantiles. Overall scores are additive scores for R and L lung and mediastinum region.

ever, comparison of PET scores and histopathology scores by lung region was far less exact in this animal model. This may reflect the limited resolution of the clinical PET scanner used in our study in this relatively small animal model. While the rabbit is of sufficient size to resolve PET features between the general lung field and nonlung areas, the lung lobes cannot be distinguished, and features near the mediastinum sometimes cannot be definitively localized in the images. Because of this resolution factor, lower sensitivity for specific lung regions than for the whole animal was not unexpected. Nonetheless, some specificity of PET imaging for diseased lung regions was shown by the low percentages of positive PET scores with negative fibrosis for the R and L lung regions.

TABLE 2
Distribution of Positive PET Scores and Histopathology Scores

	Histopathology score (positive = score > 1)	
	Negative	Positive
PET score (positive = any score > 1)		
Whole animal		
Negative	9 (90% specificity)	0
Positive	1	18 (100% sensitivity)
R lung		
Negative	12	5
Positive	1	10
L lung		
Negative	11	4
Positive	1	12
PET score (positive = any score > 2)		
Whole animal		
Negative	10	0
Positive	0	18
R lung		
Negative	13	6
Positive	0	9
L lung		
Negative	12	4
Positive	0	12

PET scores for R and L lung include mediastinum.
Histopathology scores are positive if severity and distribution were both >1. Scores for R and L lung include azygous lobe.

Another cause of error in localizing PET activity to specific lung lobes was the possibility of animal movement during imaging. Animals were sedated and observed movement was minimal, but respiration would cause some small loss of resolution. Fusion of transmission and emission images helped to localize the site and extent of the PET image feature. High-resolution scanners built for small animal studies, the use of a larger animal model, or clinical imaging, should result in improved anatomical localization of the tracer and thus to increased values for localized sensitivity and specificity.

The marginal correlation between increasing PET scores and increasing histopathology scores for silicotic animals may result from the fact that only a single dose value of dust was used for every silicotic animal. And it may represent a limitation of subjective consensus scoring of the PET image features. As a limited test of the subjective scoring of the PET images, reader-assigned abnormalities in a limited number of animals were verified by comparison with background using digital voxel data for emission activity, as described above. The results indicated that reader-identified abnormalities on visual analysis generally corresponded to quantitative uptake indices.

PET images the active disease-related metabolic process, while histopathology identifies existing anatomical fibrotic lesions, which may or may not be progressing. There was no significant change over time in the median PET scores for either silicotic or control animals. This was not a surprise for the control animals; but the constancy of PET scores over time in silicotic animals is interesting. For animals imaged more than 1 time, there is the possibility of fibrogenic activity at earlier imaging sessions resolving by the

last imaging date. That would leave an inactive fibrotic scar that could be seen by the histopathological examination that followed the last imaging, with no commensurate PET activity. A possible indication of this is seen if PET scores from all imaging sessions for an animal are considered; in that case, the measured sensitivity increases for both lung regions, but specificity decreases. A full exploration of this would appear to require a higher-resolution animal model–imager system; and inactivation of lesions would likely be seen over a longer time than the 5 mo used here.

The second fundamental question facing the use of FP PET imaging to evaluate pulmonary fibrosis is: How specific is the heightened uptake of proline or proline analog to fibroblast synthesis of collagen, since pulmonary response to silica or silicate dusts can involve both inflammation and fibrogenesis? FDG uptake was observed by PET imaging in the lungs of rabbits with experimental pneumonitis induced by *Streptococcus pneumoniae* and by bleomycin; and parallel ^{3}H-deoxyglucose autoradiography found the uptake to be localized to neutrophils associated with the inflammatory response (*24*). PET FDG measurements showed increased regional pulmonary glucose metabolism in 6 of 7 histologically proven sarcoidosis patients, which resolved as high-dose cortico-steroid therapy returned serum angiotensin-converting enzyme levels to normal (*25*). We currently are analyzing histopathology scores for inflammatory response in this animal model FP PET study. Is the FP proline analog uptake in silicosis specific to fibroblast synthesis of collagen, much as the exacerbated uptake of FDG in bleomycin-challenged rabbits was specific to neutrophil activity in the inflammatory response? There is extensive literature on animal models of silicosis in which autoradiographic analysis located tritiated or ^{14}C-labeled proline at the alveolar interstitial sites of fibroblast collagen synthesis (*26*); this suggests that a major fraction of the proline analog is taken up by direct association with collagen synthesis in fibrosis. However, the relative amounts associated with collagen synthesis and with generally heightened metabolism associated with inflammatory response is not clear. A definitive answer may require either a biochemical assay of the fractional amount of FP sequestered in the lungs as procollagen, similar to the study of protein sequestration of FP in mouse osteosarcomas (*12*), or an autoradiographic study of the microanatomical location of the accumulated FP, i.e., in pulmonary interstitial fibroblasts or in alveolar neutrophil or macrophage inflammation-associated cells. We are attempting an autoradiography study using tritiated proline and FP to determine relative levels of uptake in alveolar lumen and interstitial cellular locations. If additional studies confirm a high accuracy of FP PET imaging in detecting early fibrosis, it potentially could be useful in the diagnosis of interstitial lung fibrosis, collagen diseases, and several occupational and toxicity-related disorders.

CONCLUSION

The results of this study indicate that a significant FP PET score is correlated, with high sensitivity and specificity, with the presence of pulmonary fibrosis induced by a single instillation of silica dust in a rabbit model of silicosis in a short time period of 1 to 5 months after dust challenge. It appears that the small animal model and the resolution of the clinical PET imaging system used limited these high values to correlations over the whole lung field. FP PET imaging appears to have the potential sensitivity to detect active fibrosis in silicosis, and this may be applicable to other lung diseases, such as interstitial lung fibrosis, asbestosis, cryptogenic fibrosing alveolitis, and sarcoidosis. However, the question of specificity for detection of pulmonary fibrosis needs to be evaluated, i.e., the potential for false-positive evaluations associated with potential FP uptake by transient inflammatory processes in the lung.

ACKNOWLEDGMENTS

The NIOSH authors particularly wish to thank the personnel of the PET Center and the Animal Facilities of the West Virginia University, Robert C. Byrd Medical Center, for their collaboration in this study. We thank Dr. Val Vallyathan, Donna L. Pack, Patsy A. Willard, and Dean Newcomer of NIOSH, and Dr. Alan Ducatman of WVU, for their assistance. This study was partly funded by the central grant received from West Virginia University.

REFERENCES

1. National Institute for Occupational Safety and Health. Work-related lung disease surveillance report: 1999. DHHS/NIOSH Pub. No. 2000–105. Cincinnati, OH: NIOSH; 1999.
2. Castranova V, Vallyathan V, Wallace WE, eds. *Silica and Silica-Induced Lung Diseases*. Boca Raton, FL: CRC Press; 1996.
3. Wagner GR, Attfield MD, Parker, JE. Chest radiography in dust-exposed miners: promises and problems, potential and imperfections. *Occup Med*. 1993;8:127–141.
4. Laurent GJ, Harrison NK, McAnulty RJ. The regulation of collagen production in normal lung and during interstitial lung disease [review]. *Postgrad Med J*. 1988;64(suppl 4):26–34.
5. McAnulty RJ, Laurent GJ. Collagen and its regulation in pulmonary fibrosis. In: Phan SH, Thrall RS, eds. *Pulmonary Fibrosis*. New York, NY: Marcel Dekker; 1995:135–171.
6. Laurent GJ. Rates of collagen synthesis in lung, skin and muscle obtained in vivo by a simplified method using [3H] proline. *Biochem J*. 1982;206:535–544.
7. Chvapil M, Eskelson CD, Stiffel V, Owen JA. Early changes in the chemical composition of the rat lung after silica administration. *Arch Environ Health*. 1979;343:402–406.
8. Kaw JL, Zaidi SH. Pathogenesis of pulmonary silicosis in rats fed stock and multi-deficient diet since weaning. *Environ Res*. 1970;3:199–211.
9. Reiser KM, Hesterberg TW, Haschek WH, Last JA. Experimental silicosis I. Acute effects of intratracheally instilled quartz on collagen metabolism and morphological characteristics of rat lungs. *Am J Pathol*. 1982;107:176–185.
10. Reiser KM, Haschek WH, Hesterberg TW, Last JA. Experimental silicosis II. Long-term effects of intratracheally instilled quartz on collagen metabolism and morphological characteristics of rat lungs. *Am J Pathol*. 1983;110:30–41.
11. Takeuchi T, Rosenbloom J, Prockop D. Biosynthesis of abnormal collagens with amino acid analogues II. Inability of cartilage cells to extrude collagen polypeptides containing L- azetidine-2-carboxylic acid or cis-4-fluro-L-proline. *Biochem Biophys Acta*. 1969;175:156–164.
12. Wester HJ, Herz M, Senekowitsch R, Schwaiger M, Stocklin G, Hamacher K. Preclinical evaluation of 4–18F fluoroprolines: diastereomeric effects on metabolism and uptake in mice. *Nucl Med Bio*. 1999;26:259–265.

13. Schuster DP. Positron emission tomography: theory and applications to the study of lung disease. *Am Rev Respir Dis*. 1989;139:818–840.
14. Rhodes CG, Hughes JM. Pulmonary studies using positron emission tomography. *Eur Respir J*. 1995;8:1001–1017.
15. Kramer EL, Divgi CR. Pulmonary applications of nuclear medicine. *Clin Chest Med*. 1991;12:55–765.
16. Dewan NA, Gupta NC, Redepenning LS, Phalen JJ, Frick MP. Diagnostic efficiency of PET-FDG imaging in solitary pulmonary nodules. Potential role in evaluation and management. *Chest*. 1993;104:997–1002.
17. Hubner KF, Buonocore E, Singh SK, Gould HR, Cotton DW. Characterization of chest masses by FDG positron emission tomography. *Clin Nucl Med*. 1995;20:293–298.
18. Kubota K, Matsuzawa T, Ito M, et al. Lung tumor imaging by positron emission tomography using C-11 L-methionine. *J Nucl Med*. 1985;26:37–42.
19. Dale, K. Early effects of quartz and titanium dioxide dust on pulmonary function and tissue. *Scand J Resp Dis*. 1973;54:168–184.
20. Dale, K. Late effects of moderate doses of quartz dust on pulmonary function and tissue. *Scand J Resp Dis*. 1973;54:231–243.
21. Dale, K. Late effects of large doses of quartz on pulmonary function and tissue: an experimental study on rabbits. *Scand J Resp Dis*. 1973;54:244–254.
22. Mazza SM. Stereospecific, semi-automated N.C.A. synthesis of cis-4-[18F]-fluoro-L-proline and trans-4-[18F]fluoro-L-proline. *J Labeled Compounds Radiopharmaceut*. 2000;43:1047–1058.
23. Hubbs AF, Castranova V, Ma JYC, et al. Acute lung injury induced by a commercial leather conditioner. *Toxicol Appl Pharmacol*. 1997;143:37–46.
24. Jones HA, Clark RJ, Rhodes CG, Schofield JB, Krausc T, Haslett C. In vivo measurement of neutrophil activity in experimental lung inflammation. *Am J Respir Crit Care Med*. 1994;149:1635–1639.
25. Brudin LH, Valind SO, Rhodes CG, et al. Fluorine-18 deoxyglucose uptake in sarcoidosis measured with positron emission tomography. *Eur J Nucl Med*. 1994;21:297–305.
26. Horai Z, Kaneda M, Kasahara S, et al. Autoradiographic studies on the experimental pulmonary fibrosis of rats after 3H-proline injection. *Experimentia*. 1972;28:42–43.

JNM The Journal of NUCLEAR MEDICINE

Cis-4-[^{18}F]Fluoro-l-Proline PET Imaging of Pulmonary Fibrosis in a Rabbit Model

William E. Wallace, Naresh C. Gupta, Ann F. Hubbs, Samuel M. Mazza, Harry A. Bishop, Michael J. Keane, Lori A. Battelli, Jane Ma and Patricia Schleiff

J Nucl Med. 2002;43:413-420.

The Journal of Nuclear Medicine is published monthly.
SNMMI | Society of Nuclear Medicine and Molecular Imaging
1850 Samuel Morse Drive, Reston, VA 20190.
(Print ISSN: 0161-5505, Online ISSN: 2159-662X)

SNMMI SOCIETY OF NUCLEAR MEDICINE AND MOLECULAR IMAGING